SYNTHETIC DATA TESTS OF 3D FULL-WAVEFIELD INVERSION FOR P-WAVE ANISOTROPIC PARAMETER ESTIMATION IN FLAT LAYERED VTI, HTI AND ORTHORHOMBIC MEDIA

H. CHANG and G.A. MCMECHAN

Center for Lithospheric Studies, The University of Texas at Dallas, 800 W. Campbell Road, Richardson, TX 75080-3021, U.S.A.

(Received February 8, 2009; revised version accepted March 12, 2009)

ABSTRACT

Chang, H. and McMechan, G.A., 2009. Synthetic data tests of 3D full-wavefield inversion for P-wave anisotropic parameter estimation in flat layered VTI, HTI and orthorhombic media. *Journal of Seismic Exploration*, 18: 249-270.

Full-wavefield inversion is developed to estimate the P-wave anisotropic parameters for VTI, HTI and orthorhombic media. With full-wavefield inversion, both the traveltime and amplitude information are utilized simultaneously. The unknowns are velocities in three orthogonal directions, the azimuth of the fast horizontal velocity, and the thickness of each anisotropic layer. This parameterization assumes elliptical anisotropy, and hence limits the inversion to near offset data. A linearized (conjugate gradient) inversion is performed, in layer stripping mode, for parameters of overlapping pairs of layers; conventional isotropic NMO provides adequate starting models. All layers are inverted as if they were orthorhombic; the inversion results reveal the actual anisotropic symmetry that is present in each layer.

The inversion is illustrated by application to synthetic data for a four-layer model containing three anisotropic symmetries (VTI, HTI and orthorhombic). Unlike traveltime-based estimations,full-wavefield inversion can recover anisotropic parameters using only surface survey P-wave data; most of the inverted parameters have errors less than two percent for noise-free data. Noise contamination leads to increasing errors with increasing depth. The standard deviations of the parameter estimates are reduced, and the azimuthal coverage is improved as the number of sources increases. The inversion results for a layer are most satisfactory when constraints provided by reflections from both upper and lower interfaces are available. Correlation analysis between the parameters reveals a strong positive correlation between depth and vertical velocity in all media, and a strong correlations between fracture orientation and horizontal velocities in HTI and orthorhombic media.

0963-0651/09/$5.00

This approach provides an alternative to the usual use of traveltimes only for anisotropic parameter estimation. It sets the stage for extending full waveform inversion to elastic, non-elliptical, anisotropic models with more complicated geometries and symmetries.

KEYWORDS: 3D, anisotropy, full-wave, inversion.

INTRODUCTION

Anisotropic velocity models are becoming more widespread because the assumption of isotropy is strongly violated in some common geological settings. Shales typically exhibit transverse isotropy with a vertical symmetry axis (VTI), for which isotropic velocity analysis usually generates the wrong vertical velocity, which results in the wrong depth, or fuzzy images during migration (Thomsen, 2002). Another example of anisotropy is a vertically fractured reservoir, which can be modeled as an HTI or orthorhombic medium. HTI is transverse isotropy with a horizontal symmetry axis; an orthorhombic medium physically represents a set of parallel vertical fractures embedded in a VTI background, or two orthogonal fracture sets in an isotropic background, or two identical fracture sets with arbitrary angle (Tsvankin, 1997a). By assuming that an HTI or orthorhombic medium is isotropic, we ignore the fracture density and orientation, both of which are important for reservoir characterization.

Thomsen (1986) describes TI media in terms of the vertical P- and S-velocities (V_{P0} and V_{S0}) and three dimensionless anisotropic parameters (ϵ, δ and γ), rather than the fundamental elastic moduli. This parameterization was generalized by Tsvankin (1997a) for orthorhombic media, by using two vertical velocities (V_{P0} and V_{S0}), seven dimensionless anisotropic parameters [$\epsilon(1)$, $\epsilon(2)$, $\delta(1)$, $\delta(2)$, $\delta(3)$, $\gamma(1)$ and $\gamma(2)$], and the azimuth of the symmetry axis. Understanding of anisotropy is advanced by this intuitive notation. Today, given a complete set of parameters, forward modeling and migration are both feasible; it is the determination of the anisotropic parameters that remains the most difficult task for any anisotropic data processing (Thomsen, 2002). Full-wavefield inversion is one option that can potentially address this issue.

Extensive research has been devoted to estimation of Thomsen's and Tsvankin's anisotropic parameters, with a focus on VTI, HTI and orthorhombic media (Tsvankin and Thomsen, 1994; Alkhalifah and Tsvankin, 1995; Tsvankin, 1997b; Grechka and Tsvankin, 1999; Al-Dajani and Alkhalifah, 2000; Le Stunff et al., 2001; Grechka et al., 2002, 2005). Most current methods are based on traveltime information of P, or of P-SV converted, waves. For example, non-hyperbolic moveout can be used to estimate anisotropic parameters from wide aperture reflection time data using (Alkhalifah and Tsvankin, 1995)

$$t^2(x) = t_0^2[1 + (x/t_0V_{PNMO})^2 - 2\eta[x/t_0V_{PNMO}]^4/\{1 + (1+2\eta)[x/t_0V_{PNMO}]^2\}] \quad , \tag{1}$$

where t_x and t_0 are two-way traveltimes for offsets x and 0 respectively, V_{PNMO} is the P-wave NMO velocity, and η is a function of ϵ and δ:

$$\eta = (\epsilon - \delta)/(1 + 2\delta) \quad . \tag{2}$$

For VTI and orthorhombic media, surface survey P-wave reflection times are sufficient to recover V_{PNMO} and η [eqs. (1) and (2)] (which are the only anisotropic parameters needed for time processing). However, if the reflectors are flat, or even mildly dipping, surface survey P-wave data are not enough to estimate the complete anisotropic parameterization [V_{P0}, $\epsilon(1)$, $\epsilon(2)$, $\delta(1)$, $\delta(2)$, and $\delta(3)$] in the depth domain. P-wave traveltime inversion can not handle the trade-off between the vertical velocity and the anisotropic parameters in VTI or orthorhombic media, if additional constraints (provided by multiple-source illumination of dipping or curved interfaces, or by P-SV converted waves) are not available (Alkhalifah and Tsvankin, 1995; Grechka and Tsvankin, 1999; Tsvankin and Grechka, 2000; Le Stunff et al., 2001; Grechka et al., 2002, 2005). However, the anisotropic parameters for an HTI medium can be successfully recovered using only the normal moveout information from wide azimuth surface survey P-wave data (Al-Dajani and Alkhalifah, 2000).

In this paper, we illustrate full-wavefield inversion to estimate depth domain anisotropic parameters for VTI, HTI and orthorhombic media. Unlike any previous methods used for anisotropic parameter estimation, we utilize both the travel time and the amplitude information simultaneously. The extra constraints provided by fitting the amplitudes enable the recovery of the anisotropic parameters using only surface survey P-wave data; no reflections from dipping or curved interfaces are required. The shape of the reflectors adds complexity to the inversion, so only flat layer models are used in this initial demonstration of feasibility. Instead of Tsvankin's parameterization to define each anisotropic layer, we use velocities in three orthogonal directions, the orientation of the fast horizontal velocity, and the depth to the bottom of the layer. Tsvankin's parameters can be calculated from our parameterization; their relationships are given in the following section.

The assumption of elliptical anisotropy which, although is not physically rigorous and cannot be observed in the field, is not critical when only near offset data are used (Tsvankin and Thomsen, 1994). This paper contains the first attempt to apply full-wavefield inversion to anisotropic parameter estimation, through which we can 1) for the first time, determine vertical velocity and anisotropic parameters simultaneously for a horizontally layered VTI or

orthorhombic models using only P-wave surface survey data, and 2) provide a new approach to estimation of anisotropic parameters for HTI and orthorhombic media.

The efficiency and simplicity of full-wavefield inversion has previously been demonstrated in isotropic models with complicated geometries (Xu and McMechan, 1995), and for viscoelastic parameter estimation in 1D layered models (Martinez and McMechan, 1991; Tiwari and McMechan, 2007). The linearized scheme used in this paper is the simplest form of wavefrom inversion, and requires that the starting parameters to be sufficiently close to the correct values that the difference between the times in the predicted and the observed data are within a half wavelength (Mora, 1989). The synthetic data tests below show that linearized inversion is adequate for anisotropic parameter estimation; thus, more complicated (non-linear) inversions were not attempted.

In the following sections, we first introduce the methodology of full-wavefield inversion, and then apply it to data for a flat-layered model containing three anisotropic (VTI, HTI and orthorhombic) layers overlying an isotropic halfspace. Through this synthetic example we show, not only that the anisotropic parameters can be estimated correctly, but also that an adequate starting velocity model can be obtained from conventional methods for isotropic media. Noise-contaminated data are also inverted and the parameter correlations are analyzed with singular value decomposition.

METHODOLOGY

In linearized inversion, it is assumed that the required parameter updates are locally linearly proportional to the misfit between the calculated and observed wavefields. The validity of the linear assumption will be demonstrated numerically in the synthetic tests below.

First we input the starting model parameters, which are estimated a priori by conventional methods, in this case, isotropic normal moveout (NMO) analysis. Then we calculate the objective function O, which is the summed squared amplitude of the residual wavefield;

$$O = \sum_{i=1}^{N} (Aob - Apr)^2 \quad , \tag{3}$$

where Apr is the predicted data, Aob is the observed data, and N is the total number of time samples. Next, through linearized inversion, updated parameters are calculated and used in the next iteration until O is minimized.

Linearized inversion

The linearized inversion solves the system of linear equations

$$AX = B \quad , \tag{4}$$

where

$$A = \begin{bmatrix} \partial s_1/\partial x_1 & \partial s_1/\partial x_2 & \cdots & \partial s_1/\partial x_n \\ \partial s_2/\partial x_1 & \partial s_2/\partial x_2 & \cdots & \partial s_2/\partial x_n \\ \vdots & \vdots & \vdots & \vdots \\ \partial s_m/\partial x_1 & \partial s_m/\partial x_2 & \cdots & \partial s_m/\partial x_n \end{bmatrix}, \quad X = \begin{bmatrix} \Delta x_1 \\ \Delta x_2 \\ \vdots \\ \Delta x_n \end{bmatrix}, \quad B = \begin{bmatrix} s_1 \\ s_2 \\ \vdots \\ s_m \end{bmatrix} . \tag{5}$$

In eq. (5), n is the total number of model parameters and m is the total number of time samples. The n elements Δx_1 to Δx_n in vector X are the n unknown parameter updates that are to be solved for. B is an m-element vector; each element in B is the amplitude difference between the predicted and the observed data at the corresponding time sample. A is the m $\times$ n Jacobian matrix, which contains the partial derivatives of the amplitude s_i (for i = 1, m) with respect to the model parameter x_j (for j = 1, n). The Jacobian matrix A is calculated using finite differencing by perturbing each of the n parameters with an infinitesmal change, followed by modeling for the n perturbed models.

With the calculated matrix A and vector B, we use conjugate gradients to solve the linear eq. (4) for parameter updates X. In the examples below, we invert for nine parameters at a time; n = 9 and vector X has nine elements.

Modeling and model parameterization

The core of the inversion is the modeling program, which simulates the seismic response of an anisotropic model. It is based on a 3D anisotropic scalar wave equation implemented numerically by finite differencing (Dong and McMechan, 1991). The scalar wave equation limits the modeling, and hence the inversion, to P (or to SH) waves.

The program uses a 3D flat-layered velocity model. Each layer is defined by five parameters:

1. P-wave velocities in three orthogonal directions. There are the fast and the slow horizontal velocities (V_{90F} and V_{90S}) and the vertical velocity V_{P0}.

2. The angle α between the fast horizontal velocity and the global horizontal x-axis. This parameter does not have any physical meaning for VTI or isotropic media, since the velocity does not change horizontally. However, for HTI and orthorhombic media, α is interpreted as the fracture orientation, since the fast horizontal P-wave travels parallel to the fractures.

3. The depth to the bottom of the layer.

A three-medium model and its parameters are shown in Fig. 1. Fig. 1a has two equal horizontal velocities, and a smaller vertical velocity; this is a VTI medium, with stratified thin layers. The angle α does not have any physical meaning in VTI media and is arbitrarily set to zero. Fig. 1b has three different velocities along three orthogonal directions; α is 29°. This is an orthorhombic medium, with a fracture set with $\alpha = 29°$ embedded in a VTI background. Fig. 1c has the vertical velocity equal to the fast horizontal velocity, and a second slower horizontal velocity; α is 60°. This is an HTI medium; physically it represents a vertical fracture set embedded at $\alpha = 60°$ in an isotropic background. This parameterization has five parameters for each layer; the relative values of the parameters determine the actual type of anisotropy.

By defining the anisotropy with three P-wave velocities instead of the elastic tensor, we assume the anisotropy to be elliptical. In terms of Tsvankin's (1997) parameterization for P-wave propagation in an orthorhombic medium (ϵ_1, ϵ_2, δ_1, δ_2 and δ_3), the elliptical assumption corresponds to $\epsilon_1 = \delta_1$ and $\epsilon_2 = \delta_2$; the S-wave parameters γ_1 and γ_2 are not relevant for this model and so are not included. The equivalent Tsvankin parameters can be calculated from our parameterization using

$$\epsilon_1 = \delta_1 = (V_{90F} - V_{P0})/V_{P0} \ ,$$

$$\epsilon_2 = \delta_2 = (V_{90S} - V_{P0})/V_{P0} \ ,$$

$$\delta_3 = (V_{90F} - V_{90S})/V_{90S} \ . \qquad (6)$$

The Tsvankin anisotropic parameters for the three-layer model are shown at the right side of Fig. 1.

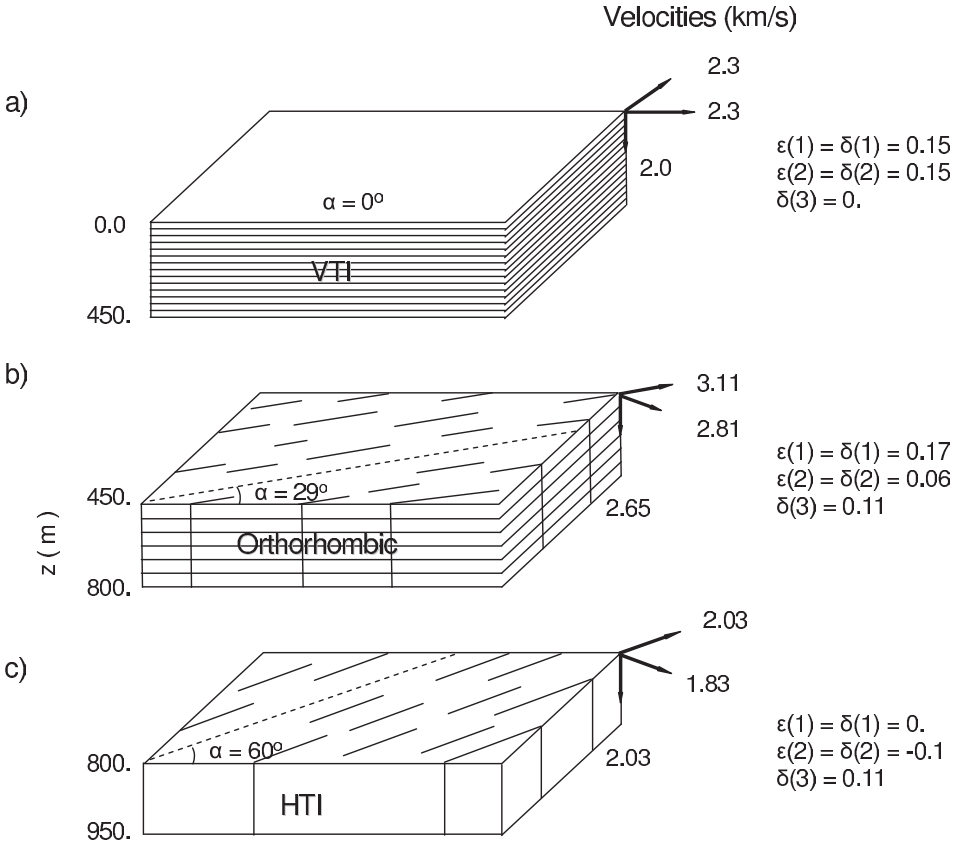

Fig. 1. The anatomy of a three-medium model; (a) is VTI, (b) is orthorhombic and (c) is HTI. The velocity orientations are denoted by the arrows and their values are labeled. The equivalent Tsvankin anisotropic parameters (at right) are calculated from our parameterization.

SYNTHETIC EXAMPLE

We apply the inversion to data from a model consisting of four flat layers (Fig. 2). The properties of the upper three layers are defined in Fig. 1. Since this is a flat-layer model, the inversion needs only one common shot gather as input, provided that the azimuthal aperture is sufficient. We simulate the observed data using the same modeling program that is used in the inversion. An explosive source with a Ricker wavelet with 12 Hz dominant frequency is located at (x, y, z) = (30,30,40) m. The receivers are on a 2D rectangular grid at the same depth as the source, and offsets in both x- and y-directions vary

from 0 to 1000 m. The receiver spacing is 10 m in both x and y directions; boundary conditions are absorbing on the sides and bottom, and a free surface on the top of the grid.

Estimating the starting parameters

For inversion, it is important to show how an adequate starting model can be built. The conventional isotropic NMO procedure is used to estimate the starting model parameters (Fig. 3a). We perform isotropic NMO analysis and Dix differentiation on two common shot line gathers [which are equivalent to common midpoint (CMP) gathers for flat layers], parallel to the x and y axis directions, respectively, to obtain approximate, apparent, directionally-dependent interval velocity functions. The results from these two orthogonal CMP lines are equal for VTI or isotropic layers, but different for HTI or orthorhombic layers. For the first (VTI) layer, the NMO result is isotropic with the wrong vertical velocity, because the estimated P-wave NMO velocity $V_{PNMO} = V_{P0} \times \sqrt{(1+2\delta)}$ (Tsvankin and Thomsen, 1994).

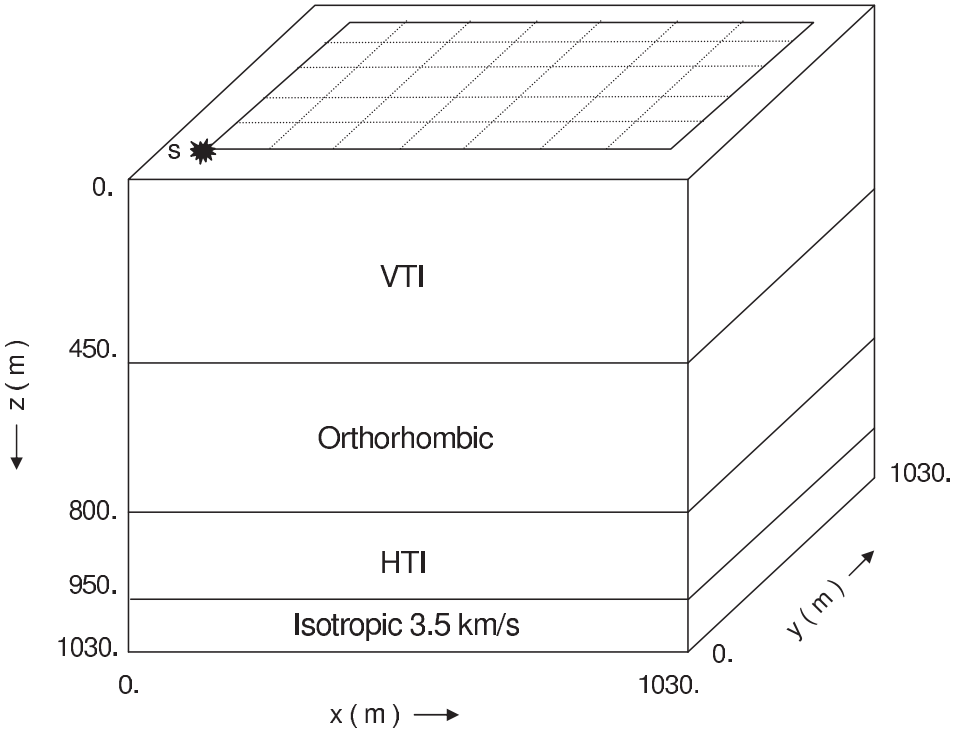

Fig. 2. Correct velocity model for the synthetic example. Details of the top three layers are shown in Fig. 1.

For the second (orthorhombic) layer (Fig. 3b), we get two different apparent velocity profiles in two directions (3.03 km/s along x and 2.87 km/s along y, denoted by the dashed arrows). Based on the NMO results, the simplest scenario we can assume for the second layer is that it is HTI with a fracture set parallel to the x direction; thus, the starting vertical velocity is set to be equal to the fast horizontal velocity (3.03 km/s).

Similarly, we can set the starting model for the third layer to be HTI with a fracture set parallel to the y direction (Fig. 3c). The dashed lines and arrows in Fig. 3b and c represent the starting model, while the solid lines and arrows are the correct values; all the parameters in the starting model have approximate, but incorrect values. For this flat-layered model, depths can be estimated from the isotropic NMO velocities as well; these depths will be incorrect because of the incorrect vertical velocities.

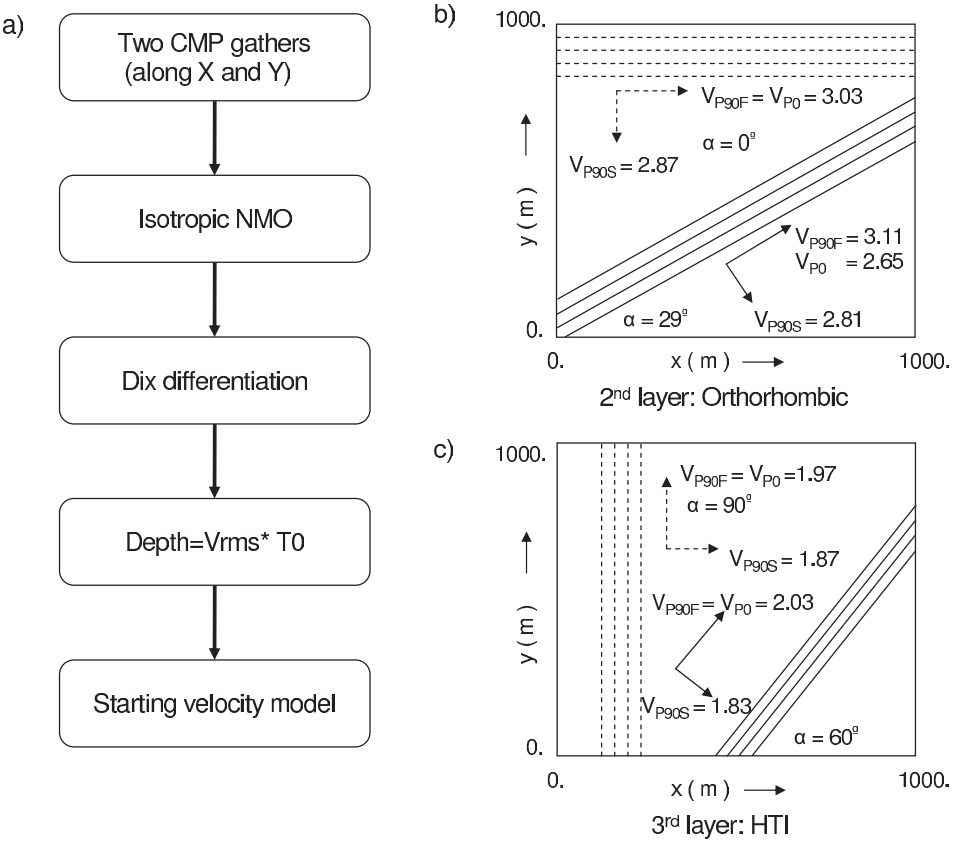

Fig. 3. The estimation of the starting model. (a) is the flow chart for the procedure; (b) and (c) show the correct model (the solid lines) and the starting model (the dashed lines) for layers 2 and 3, respectively.

Since the fourth layer is an isotropic half space, its parameters can not be estimated from NMO times alone. The starting model built from isotropic NMO guarantees that the simulated synthetic data have the correct travel times for the near offsets, so that cycle skipping can be avoided and the linear inversion can iterate toward the correct solution (Mora, 1989). We arbitrarily use the correct layer properties for the starting model of the fourth layer, and allow them to change as iterations proceed.

Layer stripping

Since each layer is defined by five parameters, the four-layer model has nineteen parameters in total. To reduce the number of unknowns at each iteration, layer stripping is used. By dividing the parameter estimation process into three separate inversions (denoted 1 to 3), the number of parameters is reduced from nineteen to nine in each inversion. Each inversion estimates the parameters of two adjacent layers; five parameters from the upper layer (V_{90F}, V_{90S}, V_{P0}, depth, and α) and four parameters from the lower layer (V_{90F}, V_{90S}, V_{P0}, and α). Both layers have two horizontal, and one vertical velocity, and the angle α, but the bottom of the lower layer does not have a defined depth. Inversion 1 estimates the parameters of layers 1 and 2, inversion 2 estimates those of layers 2 and 3, and so forth. This is the layer stripping strategy, by which the number of unknowns is limited to a minimum while still being able to solve for complicated models.

Inversion results

Inversion 1: Layers 1 and 2

Following the layer stripping strategy, we invert for layers 1 and 2 first. The starting model contains an isotropic first layer and an HTI second layer, which are obtained from isotropic NMO analysis. Since the correct model has four layers, and the first two are VTI and orthorhombic respectively (Fig. 2), the residual data between the starting and the correct models has the direct wave D and three reflections (R1, R2 and R3) from the three boundaries (Fig. 4a). If the parameters of layers 1 and 2 converge to the correct values, D and R1 should disappear while R2 and R3 should remain as constant residuals. Fig. 4 shows data extracted, from the 3D residual volume, along the representative 2D line at y = 1000 m at four different iterations. The direct wave D disappears after two iterations, but R1 is not entirely accounted for, even after seven iterations. As a result, after inversion 1, we expect the first layer to be well estimated while there is still error for the second layer. Fig. 5 shows the summed squared amplitude of the residual wavefield as a function of iteration number for layers 1 and 2; the noise-free residual is the solid line, which has a sharp drop at the first iteration, because the residual of inversion 1 is dominated by the direct wave.

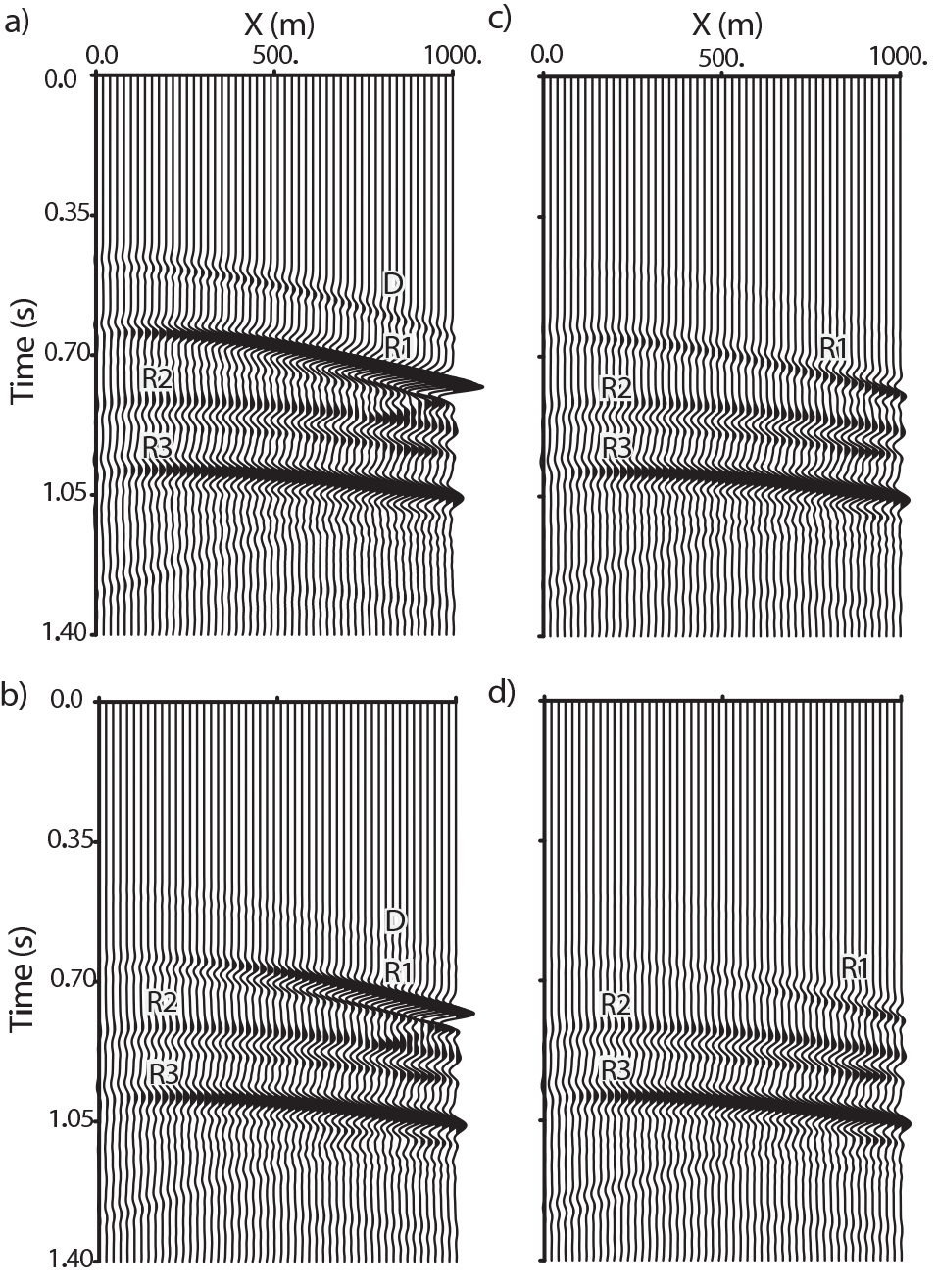

Fig. 4. Representative 2D slices at y = 1000 m extracted from the 3D residual volume before, and at different iterations of, inversion 1. (a) is the original residual before the inversion, (b) is the residual after two iterations, (c) is after five iterations, and (d) is after seven iterations. The direct wave D disappears after two iterations; the amplitude of R1 is reduced dramatically after seven iterations while R2 and R3 remain constant throughout the inversion.

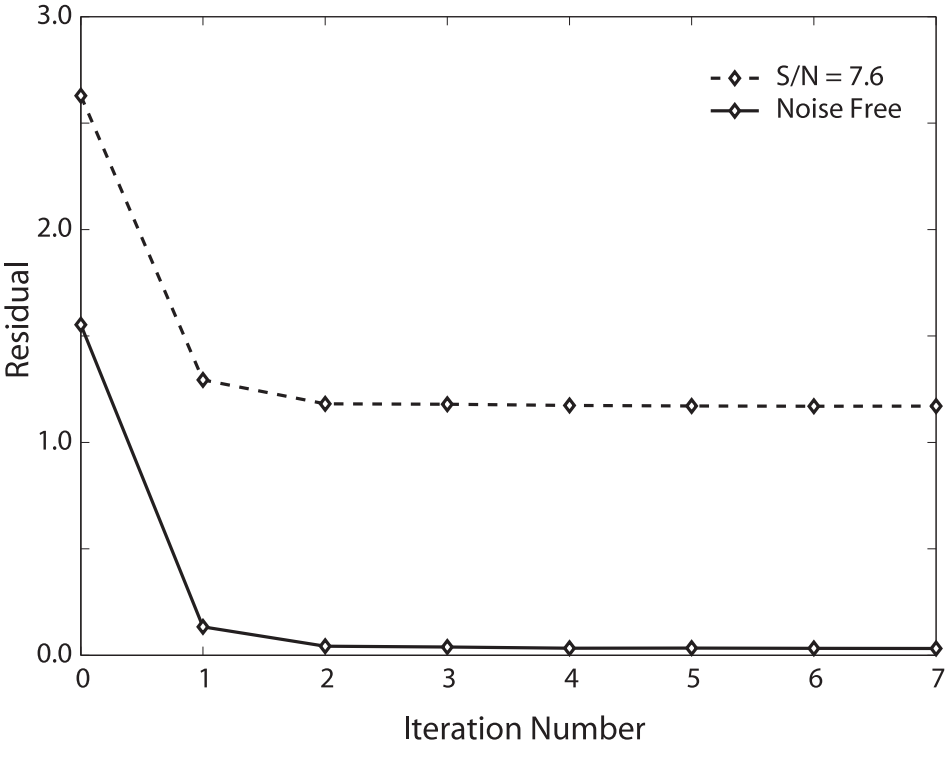

Fig. 5. Summed squared amplitude of the residual wavefield as a function of iteration number for inversion 1. Iteration 0 has the residual before the inversion. Residuals of the noise-free and lower noise level data are denoted by the solid and dashed lines, respectively.

The results from inversion 1 are in Tables 1 and 2. The layer 1 result is final, and all of its parameters converge to the correct values after seven iterations (Table 1). However, the parameters of the second layer still have errors (Table 2), which is consistent with the observed R1 residuals in Fig. 4. The less accurate result for layer 2 can be attributed to a lack of constraints. The traveltime and amplitude of D and the traveltime of R1 can uniquely determine the layer 1 properties, whereas the amplitude of R1 alone, which is the only observation that is affected by the layer 2 parameters, is not enough to recover the layer 2 parameters when layer 1 is also part of the inversion. This behavior also occurs in the next two inversions. The upper layer of each pair is always constrained by two reflections (from its top and bottom), whereas the lower layer properties contribute to only one. This is why layer stripping is used; the lower layer of one inversion is the upper layer of the next inversion, and so on. We expect to see better results for the second layer after inversion 2, for which the intermediate result in Table 2 are the starting parameters.

Table 1. Inversion result for layer 1 from inversion 1. This is also the final result for layer 1; all the parameters converge to the correct values. Tsvankin's anisotropic parameters ϵ and δ are calculated from our parameterization using eqs. (6).

Layer 1	V_{P90F} km/s	V_{P90S} km/s	V_{P0} km/s	α ^{o}	*Depth* m	$\epsilon_1 = \delta_1$	$\epsilon_2 = \delta_2$	δ_3
Starting Model	2.30	2.30	2.30	0.	520	0.	0.	0.
Inversion Result	2.30	2.30	2.00	0.	450	0.15	0.15	0.
Correct Model	2.30	2.30	2.00	0.	450	0.15	0.15	0.

Table 2. Inversion result for layer 2 from inversion 1. This interim result will be the starting parameters for inversion 2. Tsvankin's anisotropic parameters ϵ and δ are calculated from our parameterization using eqs. (6).

Layer 2	V_{P90F} km/s	V_{P90S} km/s	V_{P0} km/s	α ^{o}	*Depth* m	$\epsilon_1 = \delta_1$	$\epsilon_2 = \delta_2$	δ_3
Starting Model	3.03	2.87	3.03	0.	N/A	0.	-0.05	0.05
Inversion Result	3.13	2.77	2.57	34.	N/A	0.22	0.08	0.13
Correct Model	3.11	2.81	2.65	29.	N/A	0.17	0.06	0.11

Table 3. Inversion result for layer 2 from inversion 2. This is also the final result for the second layer. Tsvankin's anisotropic parameters ϵ and δ are calculated from our parameterization using eqs. (6).

Layer 2	V_{P90F} km/s	V_{P90S} km/s	V_{P0} km/s	α ^{o}	*Depth* m	$\epsilon_1 = \delta_1$	$\epsilon_2 = \delta_2$	δ_3
Starting Model	3.13	2.77	2.57	34.	790	0.22	0.08	0.13
Inversion Result	3.11	2.79	2.67	29.	800	0.16	0.04	0.11
Correct Model	3.11	2.81	2.65	29.	800	0.17	0.06	0.11

Inversion 2: Layers 2 and 3

In inversion 2, parameters of layers 2 and 3 are inverted by fitting R1 and R2. The starting model has three flat layers; the results in Table 2 are the starting parameters of layer 2 and the NMO interval velocity results are the starting parameters for layer 3. The parameters of layer 1 are fixed throughout the inversion. And indeed, we get a better result for layer 2 after five iterations (Table 3), compared to those from inversion 1 (Table 2). We do not show the result for layer 3, because it is an intermediate result, which again serves as the starting model for the next inversion.

Inversion 3: Layers 3 and 4

The objective of inversion 3 is to estimate the parameters of layers 3 and 4 by fitting R2 and R3. Fig. 6 shows the 2D slice at y = 1000 m from the 3D residual volume, before and after inversion 2. The residuals for R2 and R3 decrease as iterations proceed (Fig. 6). After four iterations, all the residuals are

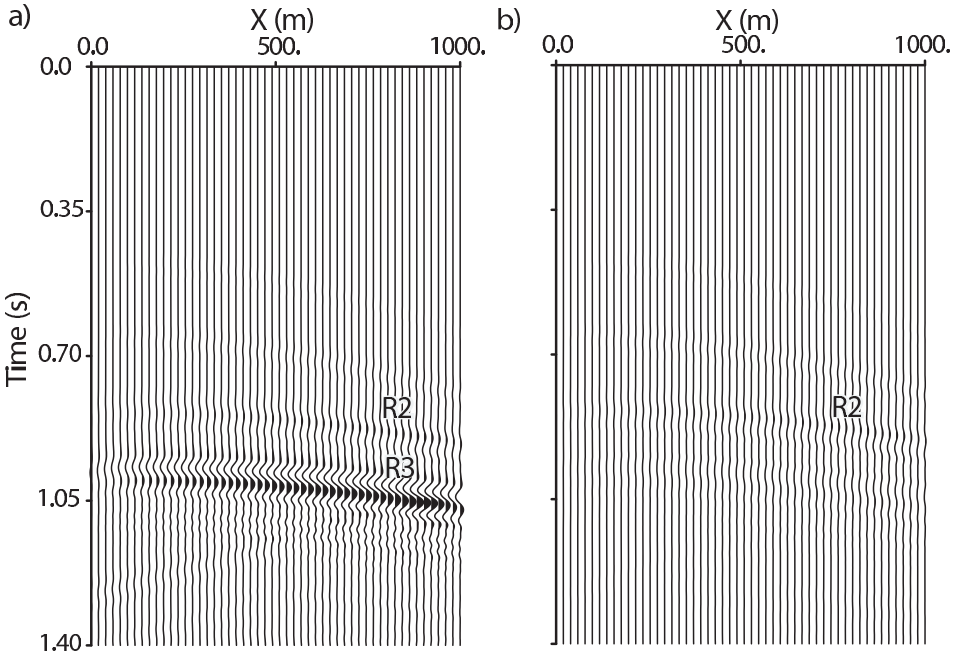

Fig. 6. Representative 2D slices at y = 1000 m extracted from the 3D residual volume at the start and end of inversion 2. (a) is the original residual before the inversion, and (b) is the residual after four iterations; (b) is minimal as expected.

mostly accounted for. Fig. 6b shows the residual wavefield between the observed data and the data simulated for the final inverted velocity model; it is minimal as expected, which indicates the successful recovery of the parameters.

Final results for layers 1 to 4

The final results for all four layers are in Table 4 (for both noise-free and noisy data). The estimated values of angle α of layers 1 and 4 in Table 4 have no physical meanings because the two estimated horizontal velocities are equal (which indicates these layers are VTI or isotropic). Compared to the correct model, the 19 parameters from the noise-free inversion results are all well fitted, and have an error less than 2%, except for the fracture angle α of layer 3, which has a 5% error. Layer 4 is fitted surprisingly well, considering that it is an isotropic half space, and is constrained only by the reflection from its top. The anisotropic/isotropic symmetries can be correctly identified from the inverted parameters.

To try to reduce the errors in inversion 2 (for layers 2 and 3), we used the inverted parameters from Table 4 as starting values, and repeated inversion 2 for all four layers; the results were not improved, thus the values in Table 4 are accepted as the solution. This synthetic test example shows that the layer stripping inversion can reasonably recover all the anisotropic parameters using only P-wave surface survey data.

Parameter correlation analysis

At the end of each inversion, we perform a singular value decomposition to get the correlations between each of the nine model parameters. Figs. 7a-c are the correlation plots for inversions 1 to 3, respectively; each parameter correlates perfectly with itself, hence the unit diagonal elements. The depth and vertical velocity of each layer are strongly positively correlated, indicated by the orange and dark red colors; this observation is consistent throughout the panels. Since each of the four layers has a different anisotropic symmetry, each has different correlation relationships between parameters. However, the orthorhombic and HTI layers (2 and 3) show strong correlations between the angle α and the horizontal velocities V_{P90F}, V_{P90S}, whereas the VTI and isotropic layers (1 and 4) do not. Also, at the end of inversion 2 (Fig. 7b), the layer 3 vertical velocity and the angle α have a positive correlation; at the end of inversion 3 (Fig. 7c) (after adding the depth parameter to the third layer), the vertical velocity is almost entirely correlated with its depth, and no longer shows any correlation with the angle α. So the information from the upper reflector alone is ambiguous, and adding constraints from the lower reflector can change the correlation relationship and improve reliability within a layer.

Table 4. Inversion results for all four layers. The four values (without brackets) for each layer for each parameter are, from top to bottom, the correct model, the noise-free inversion, the low noise (S/N = 7.6) inversion, and the high noise (S/N = 3.8) inversion results. The values in the brackets are the standard deviations of the corresponding inversion results in the same column, on the line immediately above. The angle (α) estimated for layers 1 and 4 from the noise-free data has no meaningful interpretation as the equality of V_{P90F} and V_{P90S} shows that the layers are either VTI or isotropic.

	V_{P90F} km/s	V_{P90S} km/s	V_{P0} km/s	α ^{o}	*Depth* m
Layer 1	2.3	2.3	2.0	0	450
	2.3	2.3	2.0	86	450
	2.3009	2.2997	1.9998	84	450.0
	(0.0005)	(0.0006)	(0.0004)	(26)	(0.1)
	2.3017	2.2997	1.9971	84	450.0
	(0.0010)	(0.0008)	(0.0007)	(38)	(0.2)
Layer 2	3.11	2.81	2.65	29	800
	3.11	2.79	2.67	29	800
single shot/four shots	3.1165/3.0927	2.8257/2.7726	2.6664/2.6774	26/27	800.0/800.0
	(0.0029/0.0024)	(0.0069/0.0046)	(0.0038/0.0028)	(1/1)	(0.6/0.5)
single shot/four shots	3.1160/3.1207	2.9060/2.8037	2.6574/2.6869	26/30	800.0/800.0
	(0.0058/0.0064)	(0.0124/0.0095)	(0.0069/0.0048)	(3/2)	(1.0/0.8)
Layer 3	2.03	1.83	2.03	60	950
	2.04	1.86	2.01	63	950
single shot/four shots	2.0723/2.0762	1.8364/1.8674	2.0047/2.0117	66/67	950.0/950.0
	(0.0148/0.0132)	(0.0150/0.0197)	(0.0033/0.0037)	(5/5)	(0.2/0.3)
single shot/four shots	1.8790/1.9885	1.8268/1.8301	2.0338/2.0041	34/74	960.0/950.0
	(0.0378/0.0328)	(0.0615/0.0225)	(0.0082/0.0069)	(14/17)	(0.6/0.5)
Layer 4	3.50	3.50	3.50	0	N/A
	3.53	3.53	3.52	2	
single shot/four shots	3.5649/3.5319	3.3987/3.5170	3.5008/3.5324	81/87	
	(0.0563/0.0391)	(0.0556/0.0343)	(0.0306/0.0219)	(83/74)	
single shot/four shots	3.5901/3.5378	3.4332/3.4757	3.5770/3.5469	3/5	
	(0.1116/0.0854)	(0.1247/0.0918)	(0.0582/0.0440)	(90/86)	

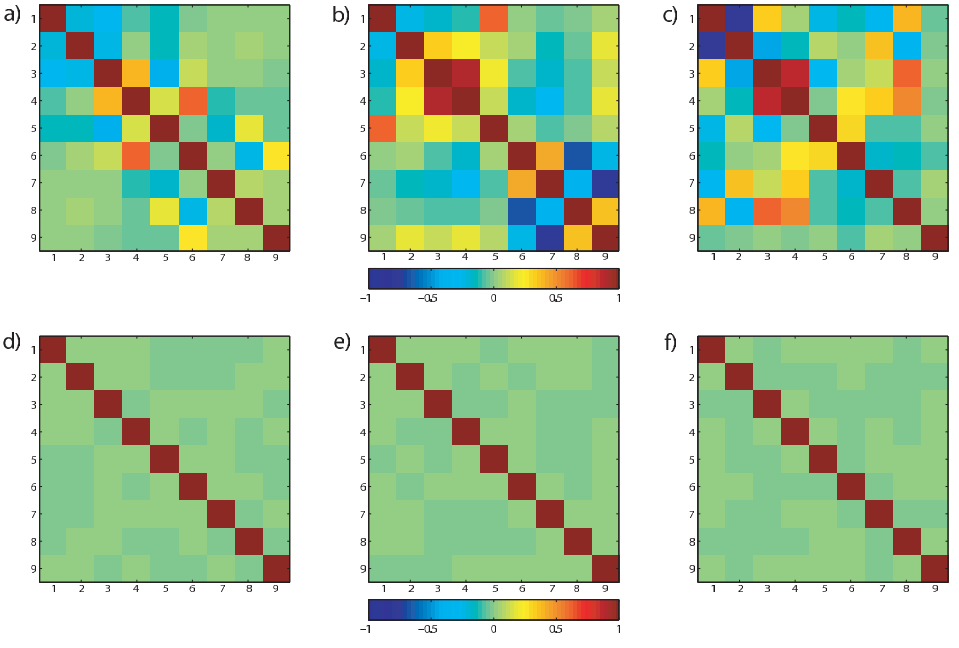

Fig. 7. The correlation and the resolution matrices. The nine anisotropic parameters within each correlation and resolution matrix, from top to bottom and from left to right, are V_{90F}, V_{90S}, V_{P0}, depth, and α for the upper layer, and V_{90F}, V_{90S}, V_{P0}, and α for the lower layer. (a)-(c) are the correlation matrices for inversions 1 to 3; (d)-(f) are the resolution matrices for inversions 1 to 3, respectively.

Figs. 7d-f are the parameter resolution matrices for inversions 1 to 3. The diagonal elements are all very close to unity because the linear systems are all over-determined [m $\gg$ n in eq. (5)]. The unit resolution matrices in Fig. 7d-f do not necessarily mean that the parameters are all well resolved; since the lower layers are not well fitted, the unity diagonal elements are primarily indicators of over-determined systems.

Noisy data

In addition to the noise-free data, two noisy datasets with different signal to noise ratios are also inverted. Fig. 8a is the noise-free data slice at y = 1000m, which is the line of receivers farthest from the source. Figs. 8b and 8c are the same slice with Gaussian noise with S/N ratios of 7.6 and 3.8, respectively. R1 and R3 are both visible at the lower noise level, but R3 is less

evident at the higher noise level. Fig. 9 shows the frequency content of both the original and the noisy data for S/N = 7.6. The original signal has a peak frequency of 12 Hz, while the noisy data has a peak frequency of 16 Hz. The frequency contents of the signal and noise overlap from 0 to 30 Hz, so the noise can not be easily removed with a frequency filter.

Table 4 shows the inversion results for the noise-free dataset and the two noisy datasets. Layer 1 parameters can be accurately recovered even at the higher noise level. During the inversion, only coherent data (the reflections) are fitted; the non-coherent noise tends to remain in the residuals (Xu et al., 1995). In Fig. 5, the shape of the residual curve of the noisy data resembles that of the noise-free data; the vertical separation between the two curves corresponds to the summed squared amplitude of the noise, and so becomes asymptotically constant with increasing iterations.

For layer 2, the inversion results from data for a single noisy shot (S/N = 7.6) have less than 5% error, except for angle α which has a 10% error (Table 4); the single shot results correctly indicate that the symmetry of layer 2 is orthorhombic. Starting from the third layer, the single shot results at the higher noise level are no longer reliable; there is a 43% error for the angle estimation, and layer 3 is indicated to be orthorhombic instead of HTI.

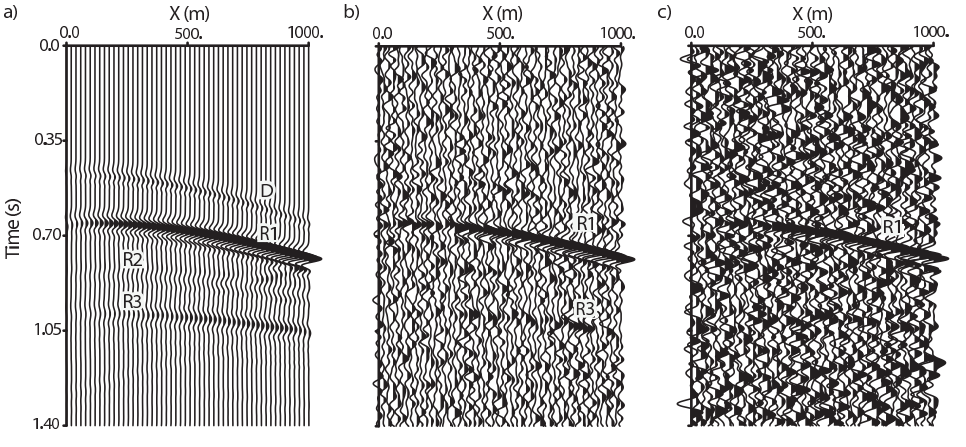

Fig. 8. Representative 2D slices at y = 1000 m extracted from the original and the noisy 3D data volumes. (a) is from the original noise-free seismic data; (b) is from the low noise data (with S/N = 7.6); (c) is from the high noise data (with S/N = 3.8).

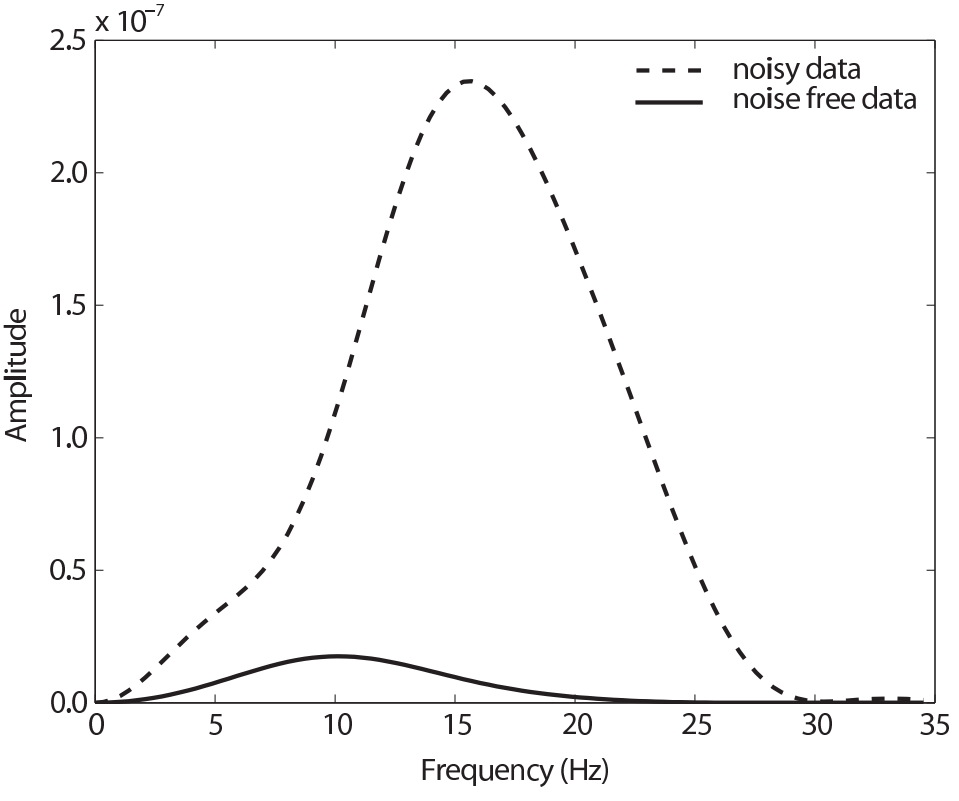

Fig. 9. Frequency content of the noisy data (with S/N of 7.6), and of the original (noise-free) seismic data. The solid line is the spectrum of the original data; it has a peak frequency of 12 Hz. The dashed line is the noisy data; its peak frequency is 16 Hz. Most of the energy is in the noise, because it is distributed throughout the time window, but the signal occurs only in narrow time ranges.

To reduce the uncertainties of the results from the noisy data, three more sources are added to the inversion; the four sources are located, one on each of the four grid corners, each with different noise having the same signal to noise ratio. Each source provides different parameter estimates that are averaged for the final solution. With multiple sources, the results are improved for every layer that has an error; especially for layers 3 and 4 (Table 4). The improvement is not surprising because the effect of averaging from four shots is similar to stacking; noise is reduced and better signal to noise ratio is obtained. Also, multiple sources provide more complete azimuthal coverage, which add independent, directionally-dependent, observations, and hence constraints, to the inversion.

The standard deviations of the inverted parameters for the noisy data are shown in brackets in Table 4. The standard deviations increase with depth, indicating the results are less reliable for the deeper layers. Since angle α has no physical meaning for the VTI and isotropic layers (1 and 4), their standard deviations are all large. The errors in the results are introduced by the errors in the data, so the standard deviations from the higher noise level (S/N = 7.6) are approximately two times of those from the lower noise level (S/N = 3.8). The poorly estimated parameters (such as the angle α of layer 3), have higher standard deviations at the higher noise level. Using multiple sources improves the results (layers 3 and 4) and reduces the corresponding standard deviations.

DISCUSSION

This is the first attempt to demonstrate the feasibility of full-wavefield inversion for anisotropic parameter estimation. The results are encouraging and suggest further research before application to field data, with focus on, but not limited to, the following areas:

1. Extension to non-elliptical anisotropy. The elliptical assumption over-simplifies the anisotropic problem; in terms of traveltime, it is not critical at the near offsets, but is increasingly inaccurate as offset increases (Tsvankin and Thomsen, 1994). Consider the following hybrid process to combine the present inversion program with non-hyperbolic moveout at far offsets (Grechka and Tsvankin, 1999) to solve for non-elliptical anisotropy. With VTI as an example, we can accomplish this in two steps; first, with full-wavefield inversion and near offset data, Vp0, δ and depth can be determined (assuming $\epsilon = \delta$, so $\eta = 0$). Then, with non-hyperbolic moveout [eq. (1)] and far offset data, η can be determined (Alkhalifah and Tsvankin, 1995). Since η is a combination of ϵ and δ [eq. (2)], ϵ can then be calculated from η and δ. This idea needs to be tested; a theoretical question is the unknown influence of the elliptical assumption on the reflection coefficient for the near offsets. This is an immediate extension with no modifications needed to the current inversion program. Alternatively, the modeling could be modified to eliminate the elliptical assumption, to invert for ϵ and δ directly using data from all offsets.

2. Extension to non-flat layers. Inversion of non-flat layered anisotropic models means more parameters in the inversion, which not only complicates the inverse problem, but also makes it more difficult to estimate the starting parameters (since there will be horizontal heterogeneity). For dipping layers, data from multiple sources have to be used to solve for the geometry coefficients. Since the present modeling program (and hence the inversion program) has the capacity for non-flat layers, this extension is straightforward in terms of software modifications. However, the influence of the extra layer shape parameters is unknown and has to be evaluated.

3. Extension to elastic inversion. Elastic anisotropy is more realistic and automatically eliminates the elliptical assumption, which is very appealing and is the longer term goal of anisotropic inversion. This extension involves replacement of the present modeling program with a 3D 3C elastic modeling program. The preferred parameterization will be Tsvankin's anisotropic parameters (because the notation is intuitive in terms of their influence on seismic responses), from which the elastic tensor can be calculated and used in the elastic modeling.

The computation cost depends on the model size and total number of time steps. For the synthetic example (with model size 103 $\times$ 103 $\times$ 103, and 1000 time steps), the run time for each (9 parameter) iteration for each shot is 3.7 minutes, using ten 2.2 GHz Opteron cluster CPUs.

CONCLUSIONS

Synthetic test examples show that full wavefield inversion can estimate all the anisotropic parameters, from P-wave surface survey data only, in a realistic number of iterations (5-7) for each layer pair. This capability is new; it is not possible if only traveltime data are used. The present version of the program is limited to flat-layer elliptically anisotropic models, but can solve for VTI, HTI and orthorhombic symmetries. Conventional isotropic NMO analysis can provide an adequate starting model for the linearized inversion. Although the inversion is capable of solving multiple-layer models, and layer stripping is a practical strategy, errors accumulate for the deeper layers. A reliable inversion for a layer needs amplitude constraints from both its top and bottom interfaces.

ACKNOWLEDGMENTS

The research leading to this paper was supported by the sponsors of the UT-Dallas Geophysical Consortium, the State of Texas Norman Hackerman Advanced Research Program under grant 009741-0021-2007,the Petroleum Research Fund of the American Chemical Society under grant 47347-AC8, and a UT-Dallas teaching assistantship. This paper is Contribution No. 1191 from the Geosciences Department at the University of Texas at Dallas.

REFERENCES

Al-Dajani, A. and Alkhalifah, T., 2000. Reflection moveout inversion for horizontal transverse isotropy: Accuracy, imitation, and acquisition. Geophysics, 65: 222-231.

Alkhalifah, T., 1997. Velocity analysis using nonhyperbolic moveout in transversely isotropic media. Geophysics, 62: 1839-1854.

Alkhalifah, T. and Tsvankin, I., 1995. Velocity analysis for transversely isotropic media. Geophysics, 60: 1550-1566.

Dong, Z.X. and McMechan, G.A., 1991. Numerical modeling of seismic waves with a 3-D anisotropic scalar-wave equation. Bull. Seismol. Soc. Am., 81: 769-780.

Grechka, V. and Tsvankin, I., 1999. 3-D moveout velocity analysis and parameter estimation for orthorhombic media. Geophysics, 64: 820-837.

Grechka, V., Pech, A. and Tsvankin, I., 2002. P-wave stacking velocity tomography for VTI media. Geophys. Prosp., 50: 151-168.

Grechka, V., Pech, A. and Tsvankin, I., 2005. Parameter estimation in orthorhombic media using multicomponent wide-azimuth reflection data. Geophysics, 70: D1-D8.

Le Stunff, Y., Grechka, V. and Tsvankin, I., 2001. Depth-domain velocity analysis in VTI media using surface P-wave data: Is it feasible?. Geophysics, 66: 897-903.

Martinez, R.D. and McMechan, G.A., 1991. Tau-p seismic data for viscoelastic media - Part 2: linearized inversion. Geophys. Prosp., 39: 157-182.

Mora, P., 1989. Inversion = migration + tomography. Geophysics, 54: 1575-1586.

Thomsen, L., 1986. Weak elastic anisotropy. Geophysics, 51: 1954-1966.

Thomsen, L., 2002. Understanding seismic anisotropy in exploration and exploitation. 2002 SEG distinguished instructor short course.

Tiwari, U.K. and McMechan, G.A., 2007. Effects of incomplete parameterization on inversion of full-wavefield inversion of viscoelastic seismic data for petrophysical reservoir properties. Geophysics, 72: 9-17.

Tsvankin, I., 1997a. Anisotropic parameters and P-wave velocity for orthorhombic media. Geophysics, 62: 1292-1309.

Tsvankin, I., 1997b. Reflection moveout and parameter estimation for horizontal transverse isotropy. Geophysics, 62: 614-629.

Tsvankin, I. and Thomsen, L., 1994. Nonhyperbolic reflection moveout in anisotropic media. Geophysics, 59: 1290-1304.

Tsvankin, I. and Grechka, V., 2000. Dip moveout of converted waves and parameter estimation in transversely isotropic media. Geophys. Prosp., 48: 257-292.

Xu, T., McMechan, G.A. and Sun, R., 1995. 3-D prestack full-wavefield inversion. Geophysics, 60: 1805-1818.